Theoretical study on the nature of Gold-X(IVA) interaction

Li Xinying (lxying@vip.henu.edu.cn)
Henan University https://orcid.org/0000-0001-9869-3543
Wanli Zhang
Henan University - Jinming Campus

Research Article

Keywords: Interaction, NBO, Topological analysis, ELF, AIM, Energy decomposition analysis

Posted Date: January 17th, 2022

DOI: https://doi.org/10.21203/rs.3.rs-1244542/v1

Abstract

Structures, stabilities, and interactions of AuX (X = C – Pb) series are theoretically investigated at CCSD(T) and B3LYP levels with extend basis sets. Natural bond orbital analysis shows that the Au-X interaction is resulted by the overlap of sp hybrid on X and 6s5d hybrid on Au atom. Laplacian and total electronic energy density values at BCP shows the “intermediate type” of Au-X (X = Si, Ge, Sn, Pb) interactions and covalent type of Au-C interaction. Moreover, analysis of electron density deformation shows pronounced charge accumulation in the middle of the region between lighter X and Au, suggesting obvious covalent character of interaction. ELF shows increased covalency from X = Pb to X = C. Energy decomposition analysis shows positive steric contribution and negative quantum contributions to the Au-X interactions. Comparing the interaction energy of AuC with other AuX series, the decrease of interaction strength between them is caused by the positive contribution of steric effect and the negative contribution of quantum and electrostatic effects. And steric energy is correlated positively with the total interaction energy and correlated positively with the steric charge deformation at BCP.

1. Introduction

Recently, gold has become the subject of a lot of attention due to gold-complex special catalysis [1–3]. Bulk metallic gold was a very poor agent for the activation of molecules, according to the configuration of outer-shell electron was $5d^{10}6s^{1}$ and its first ionization energy was 888 k J/mol [4, 5]. Due to weak adsorption ability to reactive molecules and high difficulty of bond with surface molecules, gold had no obvious catalytic activity and was generally not used as a catalyst [6]. But Haruta et al. found gold had higher catalytic oxidation activity of CO at low temperature than Pt [7, 8]. Gold gained new prominence because of its demonstrated potential as a catalyst for driving efficient and selective chemical processes [9]. The catalysis of gold-C have been extensively researched [10–14]. And it is well-established that the carbon support can influence the overall activity of gold catalysts [15]. Recently, Hong-Tao Liu and coworker investigated the nature of gold-carbon bonding in gold-alkynyl catalyst by photoelectron spectroscopy and theoretical computation uncovering an unprecedented inverse correlation between bond strength and bond orders for gold. Such strong LAu-C≡CH bonding implied that the formation of terminal alkynyl-gold was thermodynamically favorable, which was known to have important roles in alkyne activation [16]. L. S. Wang proven Si and Au form strong single covalent bonds in $SiAu_4$ cluster very close to the corresponding Si-H bonds [17]. Besides, interaction between the ligands in both metal fragments of special Au-Pb complex would favor its formation [18]. The nature of Au-complex bonding is critical to the understanding of mechanisms of gold catalysis. It is expected to be helpful to do some researches on gold catalysis by studying systematically the interaction mechanism of Au and group ⅣA atom. Our previous studies [19] have clearly demonstrated that the natural bond orbital (NBO) [20, 21], Atoms in Molecules (AIM) theory [22] and topological analysis on electron density properties, such as the electron density deformation and Laplacian are powerful utilities to explore mechanisms of interaction between atom pairs.

Reported here are the results of calculations involving AuX (X = C, Si, Ge, Sn, Pb) at the CCSD(T) theoretical level to understand nature of interaction between Au and X atom. Energy decomposition analysis (EDA)

provided by S. B. Liu [23] is used to provide quantitative research on the interaction of AuX systems.

2. Computational Details

Theoretically, that large basis set and electron correlation effect at high level are required for description of systems involved weak interaction. CCSD(T) method with large basis sets were considered [24, 25]. And the 19-valence electron ($5s^2 5p^6 5d^{10} 6s^1$) relativistic pseudo-potential and corresponding (37s33p22d2f1g)/[5s5p4d2f1g] basis sets were employed for the Au atom [26]. For C [27] and Si [28] atoms, all electron basis sets aug-cc-pVQZ were employed. The 22-valence electron relativistic pseudo-potential and corresponding (33s26p15d3f2g)/[7s6p5d3f2g] basis sets [29] were employed for Ge, Sn and Pb atoms. To obtain optimized structure of AuX system, structural optimizations were performed at the B3LYP and CCSD(T) theoretical levels by Gaussian program package [30]. Vibrational frequency analysis on the optimized geometries of selected points on the potential energy surface was carried out to determine whether the resulting geometries were true minima or transition states.

NBO analysis was performed with the NBO code of the Gaussian program [30]. Calculations of electron density properties and the energy decomposition analysis were performed by Multiwfn program [31]. And isosurface maps of various real space functions were rendered by means of Visual Molecular Dynamics (VMD) software [32].

3. Results And Discussion

Gold-contained clusters showed many special physical and chemical properties which depend strongly on the cluster size. But what attracts our attention is small clusters are more reactive than bulk materials [33]. In this section, the structures and stabilities of AuX (X = C, Si, Ge, Sn, Pb) are considered, and the interaction mechanisms between Au atom and X atoms are investigated.

3.1 Structures and stabilities

The structural parameters, binding energies (E_b), average binding energies (E_{b-ave}) of AuX systems at B3LYP and CCSD(T) methods and available experimental equilibrium structural parameters were collected in Table 1. From the table, the order of distances between Au and X computed at different level is R(B3LYP) > R(CCSD(T)); B3LYP structures accord well with the experimental values [34–36] given in parentheses, and the CCSD(T) distance is shorter than the experimental value (by about 0.18 Å). Moreover, order of the R_{Au-X} distances is $R_{Au-C} < R_{Au-Si} < R_{Au-Ge} < R_{Au-Sn} < R_{Au-Pb}$, indicating a decreased stability trend from AuC to AuPb.

Table 1
Structures and stabilities of AuX system calculated at B3LYP and CCSD(T) level.

Molecules		E_b /eV	E_{b-ave} /eV	ω /cm^{-1}	R /Å
AuC	B3LYP	4.593	2.297	673.8	1.87
	CCSD(T)	4.518	2.259	739.0	1.84
AuSi	B3LYP	4.039	2.020	362.3(400.0[a])	2.26(2.26[a])
	CCSD(T)	4.058	2.029	391.5	2.23
AuGe	B3LYP	3.772	1.886	231.8(249.7[b])	2.37(2.38[b])
	CCSD(T)	3.914	1.957	257.2	2.32
AuSn	B3LYP	3.511	1.756	181.3	2.56
	CCSD(T)	3.686	1.843	201.2	2.51
AuPb	B3LYP	3.346	1.673	148.9	2.65
	CCSD(T)	3.538	1.769	162.9	2.59
a Reference [31].					
b Reference [32].					

Besides, to understand the stability of Au-X series in detail further, E_b and E_{b-ave} values of AuX series were performed. From the Table 1, the diffidence between E_b at CCSD(T) and B3LYP level is less than 0.2 eV for AuX system. Besides, the E_b(AuC) is maximum in the AuX series, the order of E_b is E_b(AuC) > E_b(AuSi) > E_b(AuGe) > E_b(AuSn) > E_b(AuPb), AuC shows strongest stabilities among the series. From the above-mentioned comparison, for structures and stabilities of AuX systems at different computational levels, not only value of them has few differences, but trend of AuX has the same laws, B3LYP also can be used to describe AuX series.

3.2 NBO analysis

According to the NBO analysis, an AB system can be written in terms of two directed valence hybrids, h_A and h_B, on its bond enters A and B atoms, $H_{A-B} = C_A h_A + C_B h_B$. The coefficients, C_A and C_B, vary from covalent (C_A = C_B) to ionic limit (C_A >> C_B or C_B >>C_A).

For the alpha orbitals, the NBO results show one Au-C bond (BD) in AuC and it can be described mainly as $H_{Au-C} = 0.6073 h_{Au} + 0.7944 h_C$. The h_{Au} and h_C can be described as linear combination of the natural atomic orbital on its center as follows:

$$h_{Au} = 0.8954(6s) + 0.4258\left(5d_{z2}\right),$$

$$h_C = 0.3826(2s) + 0.9201\left(2p_z\right).$$

For the beta orbital, there is also only one Au-C bond in AuC system and it can be expressed as

$$H_{Au-C} = 0.7795h_{Au} + 0.6264h_C,$$

$$h_{Au} = 0.8577(6s) + 0.5033\left(5d_{z2}\right),$$

$$h_C = 0.2587(2s) + 0.9582\left(2p_z\right).$$

The results of alpha and beta orbital based on the NBO analysis suggest a polar dative bond for Au-C, closer to the covalent than the ionic. And the Au-C interaction is resulted from the overlap of a 5d6s (mainly $5d_z$) hybrid on Au atom and 2s2p (mainly $2p_z$) hybrid on C atom which can be illustrated by the natural atomic orbital occupancies in the Table 2.

Table 2
Natural population analysis (NPA) and atomic orbital occupancies at CCSD(T) level.

Mol.	NPA (Au)	Occupancy (Au)	NPA (X)	Occupancy (X)
AuC	α:0.184	$5d_{xz}^{0.941}5d_{yz}^{0.995}5d_{z2}^{0.878}6s^{0.483}6p_x^{0.01}$	-0.684	$2s^{0.941}2p_x^{0.057}2p_y^{0.990}2p_z^{0.682}$
	β:-0.050	$5d_{xz}^{0.959}5d_{yz}^{0.972}5d_{z2}^{0.895}6s^{0.702}6p_z^{0.02}$	0.550	$2s^{0.940}2p_x^{0.040}2p_y^{0.028}2p_z^{0.429}$
AuSi	α:-0.089	$5d_{yz}^{0.976}5d_{z2}^{0.960}6s^{0.618}6p_x^{0.024}6p_z^{0.009}$	-0.411	$3s^{0.951}3p_x^{0.976}3p_y^{0.021}3p_z^{0.444}$
	β:-0.050	$5d_{xz}^{0.985}5d_{yz}^{0.977}5d_{z2}^{0.96}6s^{0.612}6p_z^{0.010}$	0.550	$3s^{0.930}3p_x^{0.013}3p_y^{0.019}3p_z^{0.473}$
AuGe	α:-0.057	$5d_{xz}^{0.980}5d_{z2}^{0.964}6s^{0.584}6p_y^{0.019}6p_z^{0.009}$	-0.443	$4s^{0.958}4p_x^{0.017}4p_y^{0.981}4p_z^{0.474}$
	β:-0.081	$5d_{xz}^{0.983}5d_{yz}^{0.989}5d_{z2}^{0.966}6s^{0.63}6p_z^{0.008}$	0.581	$4s^{0.949}4p_x^{0.015}4p_y^{0.010}4p_z^{0.435}$
AuSn	α:-0.080	$5d_{xz}^{0.987}5d_{z2}^{0.975}6s^{0.589}6p_y^{0.017}6p_z^{0.009}$	-0.420	$5s^{0.958}5p_x^{0.011}5p_y^{0.983}5p_z^{0.457}$
	β:-0.112	$5d_{xz}^{0.989}5d_{yz}^{0.99}5d_{z2}^{0.976}6s^{0.641}6p_z^{0.008}$	0.612	$5s^{0.949}5p_x^{0.010}5p_y^{0.007}5p_z^{0.414}$
AuPb	α:-0.058	$5d_{yz}^{0.988}5d_{z2}^{0.976}6s^{0.568}6p_x^{0.014}6p_z^{0.010}$	-0.442	$6s^{0.964}6p_x^{0.986}6p_y^{0.010}6p_z^{0.474}$
	β:-0.159	$5d_{xz}^{0.997}5d_{yz}^{0.991}5d_{z2}^{0.98}6s^{0.685}6p_z^{0.006}$	0.659	$6s^{0.967}6p_x^{0.006}6p_y^{0.008}6p_z^{0.355}$

While for alpha orbital in AuSi system, H_{Au-Si} is represented by

$$H_{Au-Si} = 0.8126\mathrm{h}_{Au} + 0.5829h_{Si},$$

$$h_{Au} = 0.9429(6s) + 0.3280\left(5d_{z2}\right),$$

$$h_{Si} = 0.2068(3s) + 0.9742\left(3p_z\right).$$

As for the beta orbital,

$$H_{Au-Si} = 0.8197h_{Au} + 0.5728h_{Si},$$

$$h_{Au} = 0.9416(6s) + 0.3316\left(5d_{z2}\right),$$

$$h_{Si} = 0.2211(3s) + 0.9709\left(3p_z\right).$$

Combining the H_{Au-Si} of alpha and beta orbital for AuSi systems, it can be seen that the Au-Si bond is closer to the ionic than the covalent for $C_{Au} >> C_{Si}$, and the same results can be found for heavier Au-X interaction (X = Ge, Sn, Pb). And it explains that the Au-X bond in AuX system is caused by the overlap of a 5d6s (mainly $5d_z$) hybrid on Au and sp (mainly p_z) hybrid on X atom.

3.3 Electron density properties

To explore the nature of the interaction of AuX system, topological analysis of the electron density deformation, ELF, BCP properties and reduced density gradient (RDG) analysis are performed.

3.3.1 Electron Density Deformation Analysis

Figure 1 shows the electron density deformation upon the formation of AuX series. All Au and X atoms has the similar contours (or isosurfaces). Obvious blue contour lines are found in the internuclear region between Au and X, indicating that net electrons accumulate in the Au-X interaction region and showing the covalent character of AuX systems. NBO analysis indicates that the 6s and $5d_{z2}$ orbitals of the Au atom and the sp hybrid of the X atoms are crucial in Au-X interaction. Figure 1 clearly shows the charge density and charge transferred from the $6s5d_{z2}$ hybrid orbital of Au atom to the sp hybrid of X.

To get more information about charge transfer, integrated charge transfer Q(z) defined by L. Belpassi and co-workers [37] were used to measure the actual electronic charge fluctuation with respect to the isolated fragments:

$$Q\left(z_0\right) = \int_{-\infty}^{+\infty} dx \int_{-\infty}^{+\infty} dy \int_{-\infty}^{z_0} \Delta\rho(x, y, z')\, dz'$$

The point $z = z_0$ is imagined on the internuclear z axis to identify a perpendicular plane passing through that point. The corresponding value of $Q(z_0)$ is used as basis to determine the amount of charge that shifted between two planes with respect to the situation in the noninteracting fragments [37]. Negative value indicates a net charge transferred from left to right, and the difference between two Q values, $Q(z_1)$ and $Q(z_2)$, showed the net electron influx into the region delimited by two planes ($z = z_1$ and $z = z_2$). The

regions of the $Q(z_0)$ curve with a negative slope clearly corresponded to zones of charge depletion (red contours or isosurfaces in the Fig. 1), whereas charge accumulated where Q picked up (blue contours or isosurfaces in the Fig. 1).

For Au-X system, the Q value in the Fig. 2 can be both positive and negative between the Au atom and X atom, which means there are charge shifting between Au and X. According to the Fig. 2, there is a positive slope in the left region of X atoms and the increased Q in the right region of X atoms representing electron accumulation in the region. NBO analysis shows it may be caused by charge transformation of hybrid orbital. For example, as the Q curve of AuC represented, that the Q curve of AuC has a positive slope from z = -4.06 to z = -2.16 indicates net charge accumulation, which may be mainly caused by the charge transferred from the Au atom to the $2p_z$ orbital of C atom; and it leads to a negative slope, charge starts to lose rapidly until approximately z = -1.47, the charge loss may be the result of the electron loss of 2s, $2p_x$, and $2p_y$ orbitals resulted by the sp hybrid. Net charge acquired an increase from z = -1.47 to z = -0.69 and from z = -0.43 to z = 0.51, which is for the electron enhancement of 6s orbital resulting from the 5d6s hybrid. One can obtain the Q plots of all AuX have the similar trend in Fig. 2. Moreover, from Fig. 2, one can acquire that there is a positive slope between Au and X atoms, suggesting there are net electron accumulation among the interaction region between Au and X atoms (blue isosurface or contour line, Fig. 1). For Au-X system, there are pronounced electron accumulation in the middle of the region between the X and Au nuclei, suggesting the covalent character of Au-X interaction.

3.3.2 AIM

According to AIM theory from Bader [22], the interaction type can be characterized by the existence of a (3, -1) type of critical point (BCP) and the corresponding bond path. And the information about the interaction strength can be proposed by electron density properties at BCP. Generally, positive Laplacian value suggests shared-shell interactions, negative Laplacian value indicates closed-shell interaction. However, it fails to determine the types of the interaction involved heavier atoms [38–42]. D. Cremer et al. propose dual parameters, local energy density $E(r)$ and Laplacian, to distinguish between covalency and ionicity for heavy-atoms-series [43]. The 'intermediate type' of interaction can be represented by positive Laplacian $\nabla^2\rho(r)$ and negative $E(r)$ [44].

From Table 3, for AuC at CCSD(T) level, $\nabla^2\rho(r) \approx 0$, while the value of $\rho(r)$ is large enough, taking the binding energies in the Table 1 into consideration, the interaction can be classified as the covalent type. For the other AuX (X = Si - Pb) systems, Laplacian $\nabla^2\rho(r)$ is positive and $E(r)$ is negative, we can classify the interaction of them as intermediate type. By comparing the computational results of AIM at different theoretical level, the B3LYP AIM analysis also can obtain the same result of the interaction type between Au and X atoms.

Table 3
BCP properties at B3LYP and CCSD(T) level.

BCP		E	$\nabla^2\rho$	ρ	λ_2	ELF
Au-C	B3LYP	-0.137	0.050	0.193	-0.277	0.608
	CCSD(T)	-0.166	-0.005	0.212	-0.312	0.642
Au-Si	B3LYP	-0.067	-0.019	0.094	-0.088	0.452
	CCSD(T)	-0.070	0.041	0.099	-0.102	0.364
Au-Ge	B3LYP	-0.040	0.071	0.089	-0.077	0.442
	CCSD(T)	-0.050	0.067	0.098	-0.088	0.448
Au-Sn	B3LYP	-0.025	0.102	0.073	-0.057	0.343
	CCSD(T)	-0.031	0.113	0.080	-0.064	0.341
Au-Pb	B3LYP	-0.019	0.117	0.068	-0.054	0.310
	CCSD(T)	-0.025	0.130	0.076	-0.062	0.316

To quantitatively analyze electrons distribution in the basins, the localization index (LI) and delocalization index (DI) were performed by integrating electron density,$\mathrm{N}_{\Omega_i} = \int_{\Omega_i} \rho(r)\, dv$. LI measures how many electrons are localized in a basin in average, the number of electrons shared or exchanged between two atoms or basins are measured by DI.

Comparing DI(Au-X) in AuX systems, DI(Au-C) in Table 4 is the largest in all AuX systems, indicating the phenomenon of electrons accumulation in AuC system is more obvious than other AuX systems, the result is consistent with AIM analysis. For AuX(X = Si, Ge, Sn, Pb) systems, although DI(Au-Si) is the smallest, ratio between DI(Au-X) and P(Au-X) decreases from AuC to AuPb, suggesting the strength of electrons accumulation is on the wane considering the total electron population of AuX systems.

Table 4
The DI and LI of AuX systems.

Molecules	DI (Au-X)	LI(Au)	LI(X)	P(Total)	DI / P %
AuC	1.693	18.137	5.167	24.997(25)	6.773
AuSi	1.285	19.067	12.600	32.952(33)	3.900
AuGe	1.395	18.727	20.877	40.999(41)	3.403
AuSn	1.329	18.773	20.898	41.000(41)	3.241
AuPb	1.320	18.727	20.953	41.000(41)	3.220

3.3.3 Electron Localization Function.

ELF, a three-dimensional real space function within the range of (0,1), is used to describe the efficient of the Pauli repulsion at a given point of the molecular space [21]. A large ELF value usually means that it has high possibility to find an electron or a pair of localized electrons in the corresponding region. To have a better understanding of the Au-X interaction mechanism, colorfilled maps of ELF for the AuX system were depicted in the Fig. 3.

As shown in Fig. 3, there is a valence basin between Au and C atom, the ELF value is large enough and about 0.80, which suggests high possibility to find electron accumulation in the corresponding region and covalent character of interaction between Au and C. For AuSi and AuGe, although there also are valence basin, the ELF value is about 0.65 and 0.55 and it's not large enough only indicating the interaction of them contains covalent components, the interaction type of AuSi and AuGe can be thought as an intermediate type. The ELF value of Aasen and AuPb are less than 0.5, representing that the interaction in the corresponding region is closer to ionicity than covalency. ELF value between Au and X atoms decreases stepwise from AuC to AuPb, suggesting the covalency is on the wane from AuC to AuPb.

3.3.4 RDG.

To investigate the weak interactions in real space, Yang and co-workers proposed reduced density gradient (RDG) function based on the electron density and its derivatives [45], $RDG = 1/(2(3\pi^2)^{1/3})|\nabla\rho|/\rho^{4/3}$. Plots of the RDG versus sign(λ_2)ρ can analyze and visualize a wide range of interaction types. Large, negative value of sign(λ_2)ρ is indicative of stronger attractive interactions (spikes in the left part in Fig. 4), while if it is large and positive, the interaction is repulsive (spikes in the right part in Fig. 4) [45].

It is clearly shown in Fig. 4 that the line of RDG = 0.2 crosses only the attractive interaction spikes, while the line of RDG = 0.4 crosses both the attractive and the repulsive spikes. For the surface of AuPb as an example, in the first case (RDG = 0.2 isosurface), the low-density, low gradient region corresponds to the interaction region between Au and Pb atoms. The blue region clearly shows the stronger attractive interaction between Au and Pb. The RDG = 0.4 isosurface clearly shows the steric repulsion by the red loops. The electron density value at the peak itself provides the information about the interaction strength. The electron density value at the peaks of Au-X interactions decreases from about 0.212 in AuC to about 0.076 in AuPb, indicating the covalent character in the Au-X interaction and the attractive interaction strength decreases from Au-C to Au-Pb.

3.4 Energy decomposition analysis (EDA)

In a new perspective of energy decomposition proposed by S. B. Liu [23], it is found interaction energy (E_b in Table 5) can also be decomposed as E_s, E_e, and E_q, where E_s, E_e, and E_q stand respectively for the independent energy contribution from the steric, electrostatic, and quantum effect. Quantum effect [46, 47] comes from the Pauli exclusion principle (Fermi hole) [48] and dynamic electron correlation effect (Coulomb hole) [49]. Electrostatic effect mainly comes from the electron-electron, nuclear-nuclear Coulomb repulsions and nuclear-electron Coulomb attraction. Steric effect originates commonly from the fact that there will exist hindrance when each atom in a molecule is brought together.

Table 5
The total interaction energy and its partition at B3LYP level.

Molecules	E_s /eV	E_e /eV	E_q /eV	E_b /eV
AuC	26.538	-2.842	-19.103	4.593
AuSi	16.805	-1.341	-11.424	4.039
AuGe	15.687	-0.692	-11.222	3.772
AuSn	14.400	-1.008	-9.882	3.511
AuPb	14.149	-1.139	-9.664	3.346
C_2	43.364	13.474	-47.113	9.726

From Table 5, one notice that the interaction energy between Au and X atoms comes from the negative contribution of quantum and electrostatic interaction, with the latter much smaller in magnitude, indicating that the negative contribution to E_b mainly comes from the quantum effects, and positive contribution to E_b is mainly caused by steric effects. Value of E_b(AuX) and E_s(AuX) decrease from AuC to AuPb, interaction strength and steric effects between Au and X atoms decrease from X = C to X = Pb. And steric effects are attractive to the interaction between Au and X atoms. Equally, quantum repulsion and electrostatic repulsion between Au and X atoms also decrease from AuC to AuPb. Comparing AuC with other AuX series, E_b(AuC) > E_b(AuX), the interaction decrease from AuC to AuPb is mainly caused by the positive contribution of steric effect and the negative contribution of quantum and electrostatic effects. Comparing C_2 with AuC, the E_b(AuC) < E_b(C_2), meaning the interaction strength decreases, and the interaction decrease mainly comes from the positive contribution of steric and electrostatic interaction and the negative contribution of quantum interaction. It may indicate that the interaction decrease is caused by steric effect decrease and compensated by quantum effect increase for AuX series.

To get more information about steric effects in the formation of AuX, steric charge provided by S. B. Liu and co-workers is used as a local descriptor to quantitatively describe steric effects [50]. The steric charge distribution of single atom and AuX series at B3LYP level can be visualized from Fig. 5 and Fig. 6. Steric charge distribution of single atom is symmetrical from Fig. 5. The most of AuX steric charge distributions localize near the nuclei. And one notice that isosurface shape of AuSi and AuPb had smaller change than AuC, indicating the interaction type between Au and X atoms may cause effects to the steric charge distribution. And it suggests steric effect provide positive contribution to the interaction decrease. The steric charge deformation ($\triangle e_s$) at BCP was performed at B3LYP level. According to Fig. 7, E_s(AuX) increases from X = C to X = Pb, but $\triangle e_s$(AuX) decreases stepwise. E_s(AuX) is positively correlated with $\triangle e_s$(AuX) and the E_s is higher and the steric charge shift is more obvious at the BCP, also indicating that the E_s does positive contribution to the Au-X interaction.

4. Conclusions

1. Systematic CCSD(T) investigations on AuX (X = C, Si, Ge, Sn, Pb) series gave structures, stabilities, and insights into the mechanism of Au-X interactions.

a) NBO analysis suggests the overlap of sp hybrid on X and 6s5d hybrid on Au atom, moreover, the analysis of NPA and atomic orbital occupancy pictured the charge transfer mechanism, and the charge transferred from 6s and 5d orbitals of the Au atom to the p orbital of C atom. While the charge transferred from the sp orbital of X (X = Si-Pb) atoms to the 6s and 5d orbitals of Au atom.

b) Analysis of electron density deformation and integrated charge transfer Q(z) show obvious charge accumulation in Au-C interaction region, suggesting pronounced covalent character.

c) Positive Laplacian values and negative total electronic energy density values at BCPs show the “intermediate type” character of AuX (X=Si-Pb) interactions. Large electron density values indicate the covalent character of AuC. Analysis of ELF indicated the covalency decrease from X = C to X = Pb.
2. Energy decomposition analysis on Au-X interaction energy are performed to quantitatively evaluate contribution from steric effects, quantum effects and electrostatic effects.

a) The energy decomposition analysis shows interaction between Au and X atoms is mainly caused by steric attraction and quantum repulsion. Moreover, steric effect and quantum effect between Au and X atoms decreases from AuC to AuPb. And interaction strength of AuC is the strongest in the AuX system. Comparing the interaction energy of AuC with other AuX series, the interaction energy decrease is mainly caused by positive contribution of steric effects and compensated by quantum and electrostatic effects.

b) Effects to steric charge distribution may be caused by the interaction type between Au and X atoms. Steric effect provides positive contribution to the interaction decrease. Moreover, E_s(AuX) is positively correlated with $\triangle e_s$(AuX), the E_s is higher, the steric charge accumulation is more obvious at the BCP, also indicating E_s(AuX) does positive contribution to the Au-X interaction.

Declarations

Acknowledgments

Supports from Natural Science Foundation of China (No. U1404210) are gratefully acknowledged.

Data Availability

The data that support the findings of this study are available from the corresponding author upon reasonable request.

Conflict of interest The authors declare no conflicts of interest.

Ethics approval The ethical standards have been met.

Consent to participate All authors consent to participate in the research.

Consent for publication All authors declare that they agree with the submission and eventual publication of this article.

References

1. Malta Grazia, Kondrat Simon A, Freakley Simon J, Davies Catherine J, Lu Li D, Simon T, Adam G, Emma K, Morgan David J et al (2017) Identification of single-site gold catalysis in acetylene hydrochlorination. Science 355:1399–1403. https://doi.org/10.1126/science.aal13439
2. Ding Dong M, Tao F, Minghao, Xuefeng J (2016) Utility of ligand effect in homogenous gold catalysis: enabling regiodivergent π-bond-activated cyclization. J Am Chem Soc 138:5218–5221. https://doi.org/10.1021/jacs.6b01707
3. Hutchings Graham J (2018) Heterogeneous gold catalysis. ACS Cent Sci 4:1095–1101. https://doi.org/10.1021/acscentsci.8b00306
4. Hammer, Bjørk, Norskov Jens K (1995) Why gold is the noblest of all the metals. Nature 376:238–240. https://doi.org/10.1038/376238a0
5. Bond Geoffrey C, Thompson David T (2000) Gold-catalysed oxidation of carbon monoxide. Gold Bull 33:41–50. https://doi.org/10.1007/bf03216579
6. Bond Geoffrey C (2002) Gold: a relatively new catalyst. Catal Today 72:5–9. https://doi.org/10.1016/s0920-5861(01)00522-3
7. Haruta Masatake K, Tetsuhiko S, Hiroshi, Nobumasa Y (1987) Novel gold catalysts for the oxidation of carbon monoxide at a temperature far below 0 ℃. Chem Lett 16:405–408. https://doi.org/10.1246/cl.1987.405
8. Hutchings Graham J, Haruta M (2005) A golden age of catalysis: A perspective. Appl Catal A: Gen 291:2–5. https://doi.org/10.1016/j.apcata.2005.05.044
9. Lu Z, Li T, Mudshinge SR, Xu B, Hammond GB (2021) Optimization of Catalysts and Conditions in Gold(I) Catalysis–Counterion and Additive Effects. Chem Rev 121:8452–8477. https://doi.org/10.1021/acs.chemrev.0c00713
10. Li W, Zhang C, Han M, Ye Y, Zhang S, Liu Y, Wang G, Liang C et al (2019) Ambient Electrosynthesis of Ammonia Using Core-Shell Structured Au@C Catalyst Fabricated by One-Step Laser Ablation Technique. ACS Appl Mater Interfaces 11:44186–44195. https://doi.org/10.1021/acsami.9b14770
11. Ruan Mingbo S, Ping L, Jing L, Erling, Xu W (2017) Highly Efficient Regeneration of Deactivated Au/C Catalyst for 4-Nitrophenol Reduction. J Phys Chem C 121:25882–25887. https://doi.org/10.1021/acs.jpcc.7b08787
12. Rodriguez José A, Liu Ping T, Yoshiro N, Kenichi V, Francesc, Francesc I (2009) Desulfurization of Thiophene on Au/TiC (001): Au–C Interactions and Charge Polarization. J Am Chem Soc 131:8595–8602. https://doi.org/10.1021/ja901522a
13. Prati L, Villa A, Lupini AR, Veith GM (2012) Gold on carbon: one billion catalysts under a single label. Phys Chem Chem Phys 14::2969–2978. https://doi.org/10.1039/c2cp23405j

14. Engel J, Francis S, Roldan A (2019) The influence of support materials on the structural and electronic properties of gold nanoparticles – a DFT study. Phys Chem Chem Phys 21:19011–19025. https://doi.org/10.1039/c9cp03066b
15. Bianchi Claudia L, Biella Serena G, Antonella P, Laura, Michele R (2003) Gold on Carbon: Influence of Support Properties on Catalyst Activity in Liquid-Phase Oxidation. Catal Lett 85:. https://doi.org/10.1023/a:1022176909660
16. Liu HT, Xiong XG, Dau PD, Wang YL, Huang DL et al (2013) Probing the nature of gold-carbon bonding in gold-alkynyl complexes. Nat Commun 4:2223. https://doi.org/10.1038/ncomms3223
17. Wang L-S (2010) Covalent gold. Phys Chem Chem Phys 12:8694–8705. https://doi.org/10.1039/c003886e
18. Lopez-de-Luzuriaga JM, Monge M, Olmos ME, Rodriguez-Castillo M, Sorroche A (2021) Computational prediction of Au(I)-Pb(II) bonding in coordination complexes and study of the factors affecting the formation of Au(I)-E(II) (E = Ge, Sn, Pb) covalent bonds. Phys Chem Chem Phys 23:10174–10183. https://doi.org/10.1039/d1cp00325a
19. Li X (2014) Metalophilic interaction in gold halide: quantum chemical study of AuX (X = F-At). J Comput Chem 35:923–931. https://doi.org/10.1002/jcc.23577
20. Reed Alan E, Weinhold F (1983) Natural bond orbital analysis of near-Hartree–Fock water dimer. J Chem Phys 78:4066–4073. https://doi.org/10.1063/1.445134
21. Becke Axel D, Edgecombe Kenneth E (1990) A simple measure of electron localization in atomic and molecular systems. J Chem Phys 92::5397–5403. https://doi.org/10.1063/1.458517
22. Bader RFW (1990) Atoms in molecules a quantum theory. Clarendon Press, Oxford
23. Liu SB (2007) Steric effect: A quantitative description from density functional theory. J Chem Phys 126:244103. https://doi.org/10.1063/1.2747247
24. Puzzarini C, Peterson KA (2005) Multiple bonds to gold: a theoretical investigation of XAuC (X= F, Cl, Br, I) molecules. Chem Phys 311:177–186. https://doi.org/10.1016/j.chemphys.2004.10.004
25. Chalasinski, Grzegorz, Szczesniak Malgorzata M (1994) Origins of structure and energetics of van der Waals clusters from ab initio calculations. Chem Rev 94:1723–1765. https://doi.org/10.1021/cr00031a001
26. Peterson Kirk A, Puzzarini C (2005) Systematically convergent basis sets for transition metals. II. Pseudopotential-based correlation consistent basis sets for the group 11 (Cu, Ag, Au) and 12 (Zn, Cd, Hg) elements. Theor Chem Acc 114:283–296. https://doi.org/10.1007/s00214-005-0681-9
27. Kendall Rick A, Dunning Thom H, Harrison Robert J (1992) Electron affinities of the first-row atoms revisited. Systematic basis sets and wave functions. J Chem Phys 96:6796–6806. https://doi.org/10.1063/1.462569
28. Dunning Thom H (1993) Gaussian basis sets for use in correlated molecular calculations. III. The atoms aluminum through argon. J Chem Phys 98:1358–1371. https://doi.org/10.1063/1.464303
29. Pritchard Benjamin P, Altarawy Doaa D, Brett, Gibson Tara D, Windus Theresa L (2019) New basis set exchange: An open, up-to-date resource for the molecular sciences community. J Chem Inf Model

59:4814–4820. https://doi.org/10.1021/acs.jcim.9b00725

30. Frisch MJ, Trucks GW, Schlegel HB, Scuseria GE, Robb MA, Cheeseman JR, Montgomery JA Jr, Vreven T, Kudin KN, Burant JC, Millam JM, Iyengar SS, Tomasi J, Barone V, Mennucci B, Cossi M, Scalmani G, Rega N, Petersson GA, Nakatsuji H, Hada M, Ehara M, Toyota K, Fukuda R, Hasegawa J, Ishida M, Nakajima T, Honda Y, Kitao O, Nakai H, Klene M, Li X, Knox JE, Hratchian HP, Cross JB, Bakken V, Adamo C, Jaramillo J, Gomperts R, Stratmann RE, Yazyev O, Austin AJ, Cammi R, Pomelli C, Ochterski J, Ayala PY, Morokuma K, Voth GA, Salvador P, Dannenberg JJ, Zakrzewski VG, Dapprich S, Daniels AD, Strain MC, Farkas O, Malick DK, Rabuck AD, Raghavachari K, Foresman JB, Ortiz JV, Cui Q, Baboul AG, Clifford S, Cioslowski J, Stefanov BB, Liu G, Liashenko A, Piskorz P, Komaromi I, Martin RL, Fox DJ, Keith T, Al-Laham MA, Peng CY, Nanayakkara A, Challacombe M, Gill PMW, Johnson BG Chen W, Wong MW, Gonzalez C, Pople JA (2003) Gaussian 03W. Gaussian Inc., Pittsburgh
31. Lu T, Chen FW (2012) Multiwfn: a multifunctional wavefunction analyzer. J Comput Chem 33:580–592. https://doi.org/10.1002/jcc.22885
32. Humphrey William D, Andrew, Klaus S (1996) VMD: visual molecular dynamics. J Mol Graph 14:33–38. https://doi.org/10.1016/0263-7855(96)00018-5
33. Pyykkö P (2007) Magic nanoclusters of gold. Nat Nanotechnol 2: 273–274. https://doi.org/10.1038/nnano.2007.119
34. Scherer JJ, Paul JB, Collier CP, Saykally RJ (1995) Cavity ringdown laser absorption spectroscopy and time-of-flight mass spectroscopy of jet-cooled copper silicides. J Chem Phys 102:5190–5199. https://doi.org/10.1063/1.469244
35. Scherer JJ, Paul JB, Collier CP, O'Keefe A, Saykally RJ (1995) Cavity ringdown laser absorption spectroscopy and time-of-flight mass spectroscopy of jet-cooled gold silicides. J Chem Phys 103:9187–9192. https://doi.org/10.1063/1.469244
36. Kingcade JE Jr, Choudary UV, Gingerich KA (1979) Stability and thermodynamics of ligand-free germanium-gold clusters. Inorg Chem 18:3094–3104. https://doi.org/10.1021/ic50201a029
37. Belpassi Leonardo I, Ivan T, Francesco, Lucas V (2008) The chemical bond between Au (I) and the noble gases. Comparative study of NgAuF and $NgAu^+$ (Ng= Ar, Kr, Xe) by density functional and coupled cluster methods. J Am Chem Soc 130:1048–1060. https://doi.org/10.1021/ja0772647
38. Macchi Piero P, Davide M, Angelo S (1998) Experimental electron density in a transition metal dimer: metal–metal and metal–ligand bonds. J Am Chem Soc 120:13429–13435. https://doi.org/10.1021/ja982903m
39. Macchi P, Garlaschelli L, Martinengo S, Sironi A (1999) Charge density in transition metal clusters: supported vs unsupported Metal–Metal interactions. J Am Chem Soc 121:10428–10429. https://doi.org/10.1021/ja9918977
40. Pan Sudip G, Ashutosh M, Subhajit M, Diego M, Gabriel, Chattaraj Pratim K (2015) Metastable behavior of noble gas inserted tin and lead fluorides. Phys Chem Chem Phys 17:972–982. https://doi.org/10.1039/c4cp03856h
41. Pan Sudip G, Ashutosh S, Ranajit M, Gabriel, Chattaraj Pratim K (2015) A coupled-cluster study on the noble gas binding ability of metal cyanides versus metal halides (metal= Cu, Ag, Au). J Comput Chem

36:2168–2176. https://doi.org/10.1002/jcc.24190

42. Novozhilova Irina V, Volkov Anatoliy V, and Coppens Philip (2003) Theoretical analysis of the triplet excited state of the $[Pt_2 (H_2P_2O_5)_4]^{4-}$ ion and comparison with time-resolved X-ray and spectroscopic results. J Am Chem Soc 125:1079–1087. https://doi.org/10.1021/ja027857b
43. Cremer D, Kraka E (1984) Chemical bonds without bonding electron density—does the difference electron-density analysis suffice for a description of the chemical bond? Angew Chem Int Ed 23:627–628. https://doi.org/10.1002/anie.198406271
44. Nakanishi Waro H, Satoko, Kenji N (2008) Atoms-in-molecules dual parameter analysis of weak to strong interactions: behaviors of electronic energy densities versus laplacian of electron densities at bond critical points. J Phys Chem A 112:13593–13599. https://doi.org/10.1021/jp8054763
45. Johnson Erin R, Keinan Shahar C, Aron J, Weitao Y (2010) Revealing noncovalent interactions. J Am Chem Soc 132: 6498-6506. https://doi.org/10.1021/ja100936w
46. Weisskopf Victor F (1975) Of atoms, mountains, and stars: a study in qualitative physics. Science 187:605–612. https://doi.org/10.2307/1739660
47. Badenhoop JK, Weinhold F (1997) Natural bond orbital analysis of steric interactions. J Chem Phys 107:5406–5421. https://doi.org/10.1063/1.474248
48. Luken William L, Beratan David N (1982) Localized orbitals and the Fermi hole. Theor Chim Acta 61:265–281. https://doi.org/10.1007/bf00550971
49. Benesch, Robert, Smith H Jr (1971) Radial Electron–Electron Distributions and the Coulomb Hole for Be. J Chem Phys 55:482–488. https://doi.org/10.1063/1.1675777
50. Liu S, Liu L, Yu D, Rong C, Lu T (2018) Steric charge. Phys Chem Chem Phys 20:1408–1420. https://doi.org/10.1039/c7cp07678a

Figures

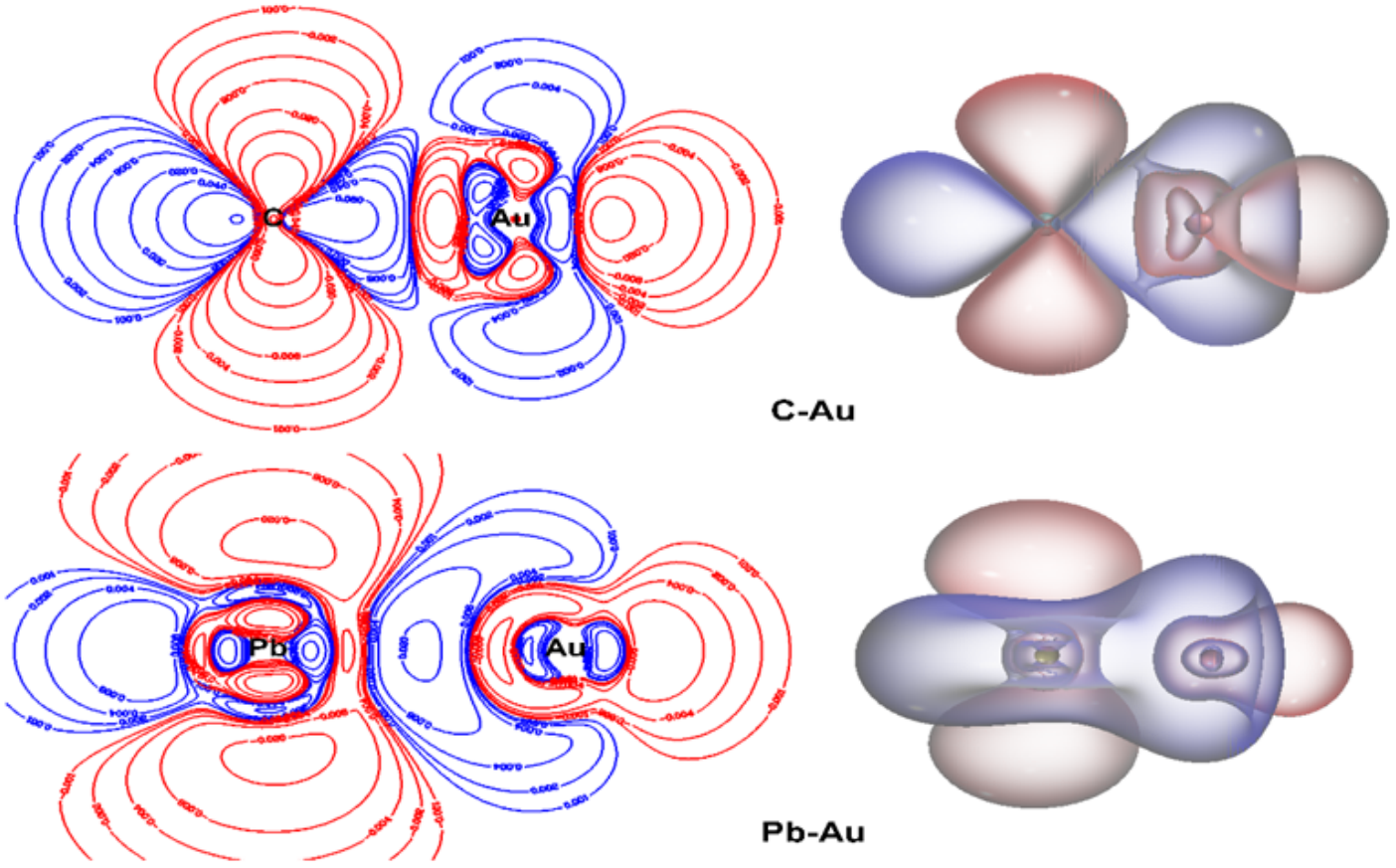

Figure 1

Contours and isosurfaces of the electron density deformation for AuC and AuPb series. Red and blue lines (isosurfaces) are in regions of the charge depletion ($\triangle\rho < 0$) and the charge accumulation ($\triangle\rho > 0$), respectively.

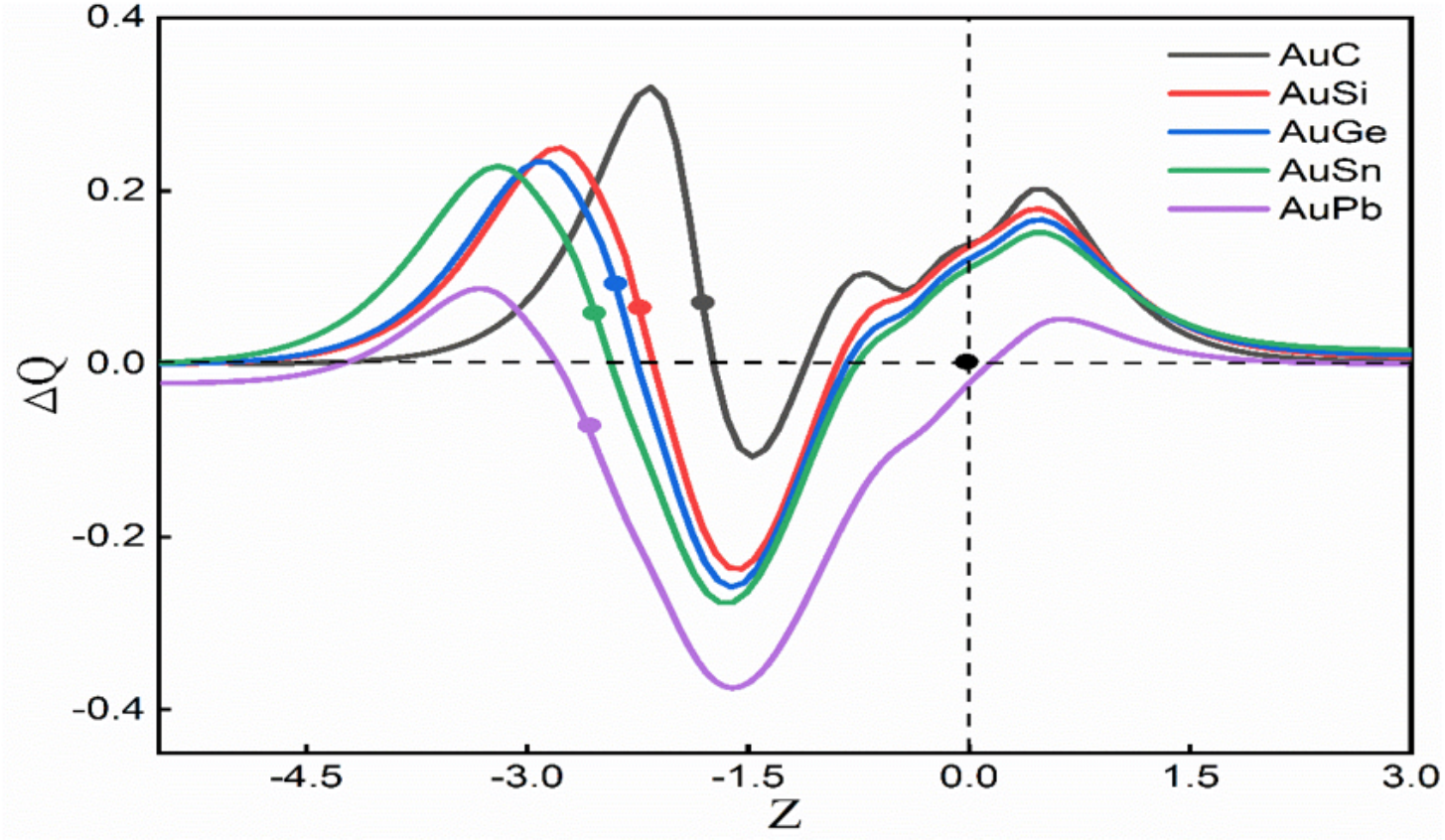

Figure 2

Integrated charge transfer as a function of the internuclear distance for the AuX system at CCSD(T) computation level. Q was calculated with the following lower and upper limits: x = [-6, 6], y = [-6, 6], z = [-6, 6]. For all systems, the Au atoms were arranged at the (0, 0, 0) site.

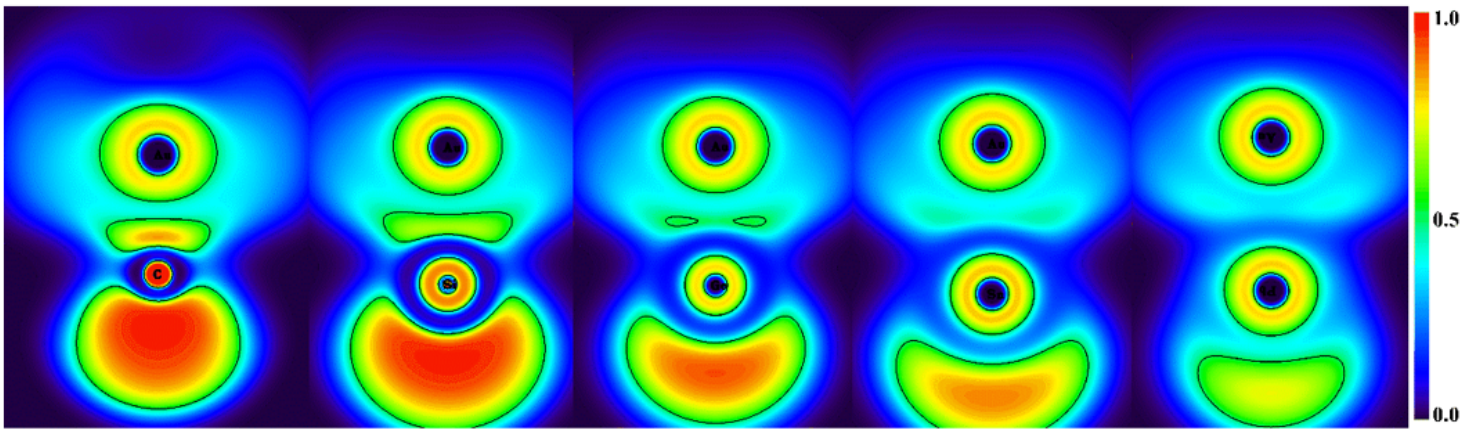

Figure 3

2D color plots of the ELF of AuX (X =C, Si, Ge, Sn, Pb). Scales [0.0, 1.0] for ELF , the value of contour lines in the figure is ELF = 0.5.

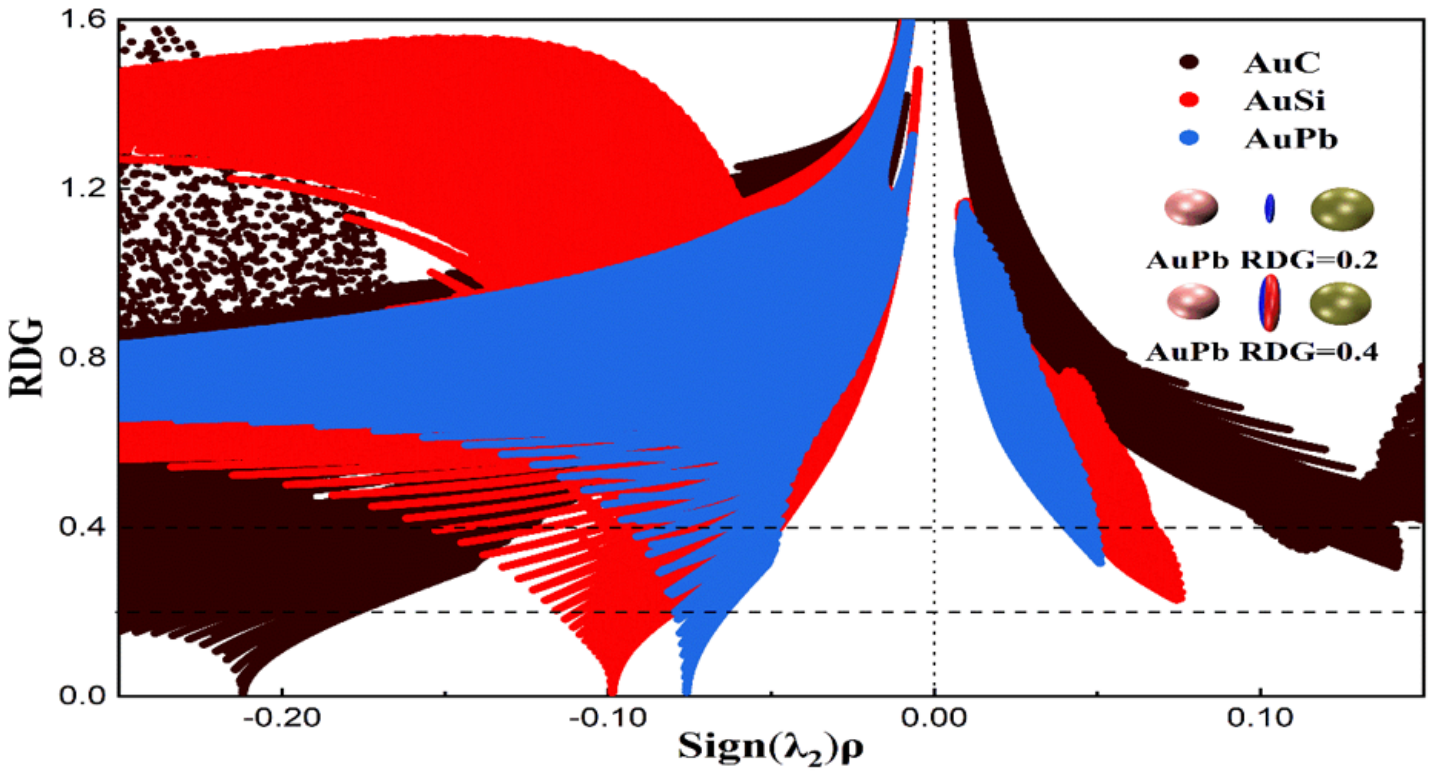

Figure 4

Plots of the RDG versus sign(λ_2)ρ and RDG isosurface (RDG = 0.2 and 0.4) for AuC, AuSi and AuPb at CCSD(T) level. The surfaces are colored on a blue–green–red scale according to values of sign(λ_2)ρ. Blue indicates attractive interactions, and red indicates nonbonding overlaps.

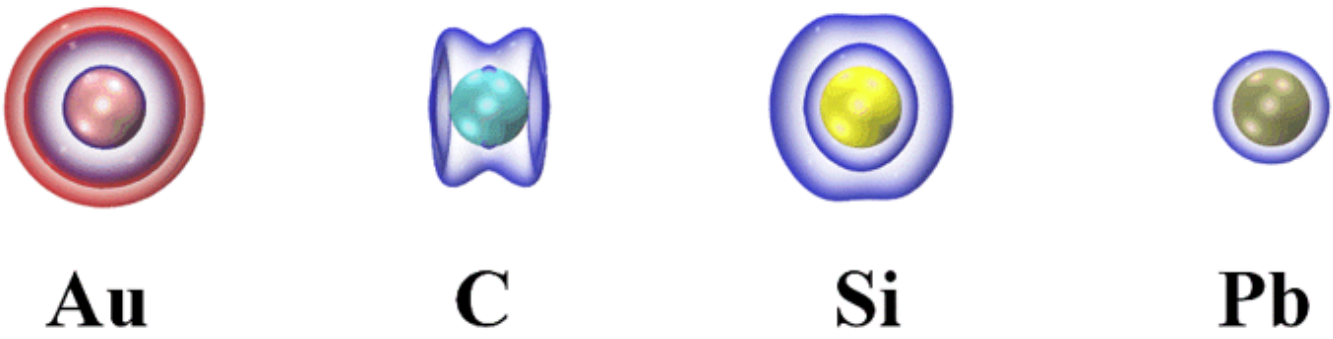

Figure 5

Contour surface of steric charge of Au, C, Si and Pb atom at 0.1 a.u. Red isosurfaces stand for a negative value and blue isosurfaces stand for a positive value.

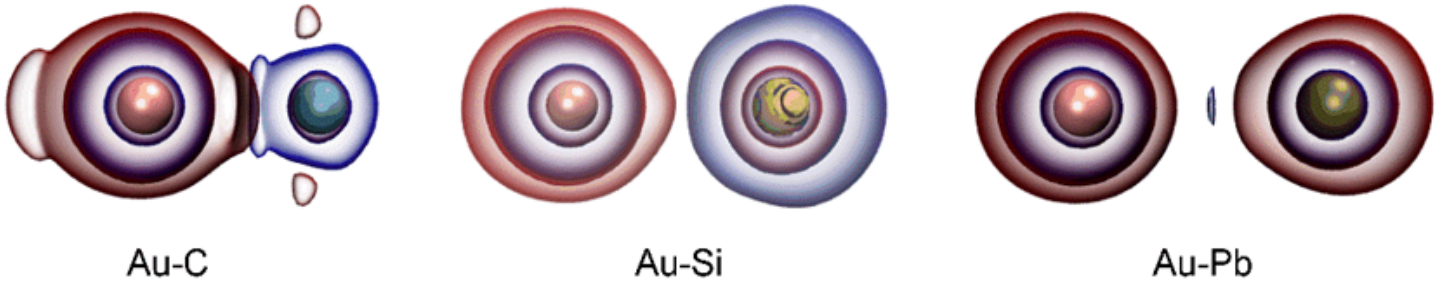

Figure 6

Contour surface of steric charge of Au-X at 0.1 a.u. Red isosurfaces stand for a negative value and blue isosurfaces stand for a positive value.

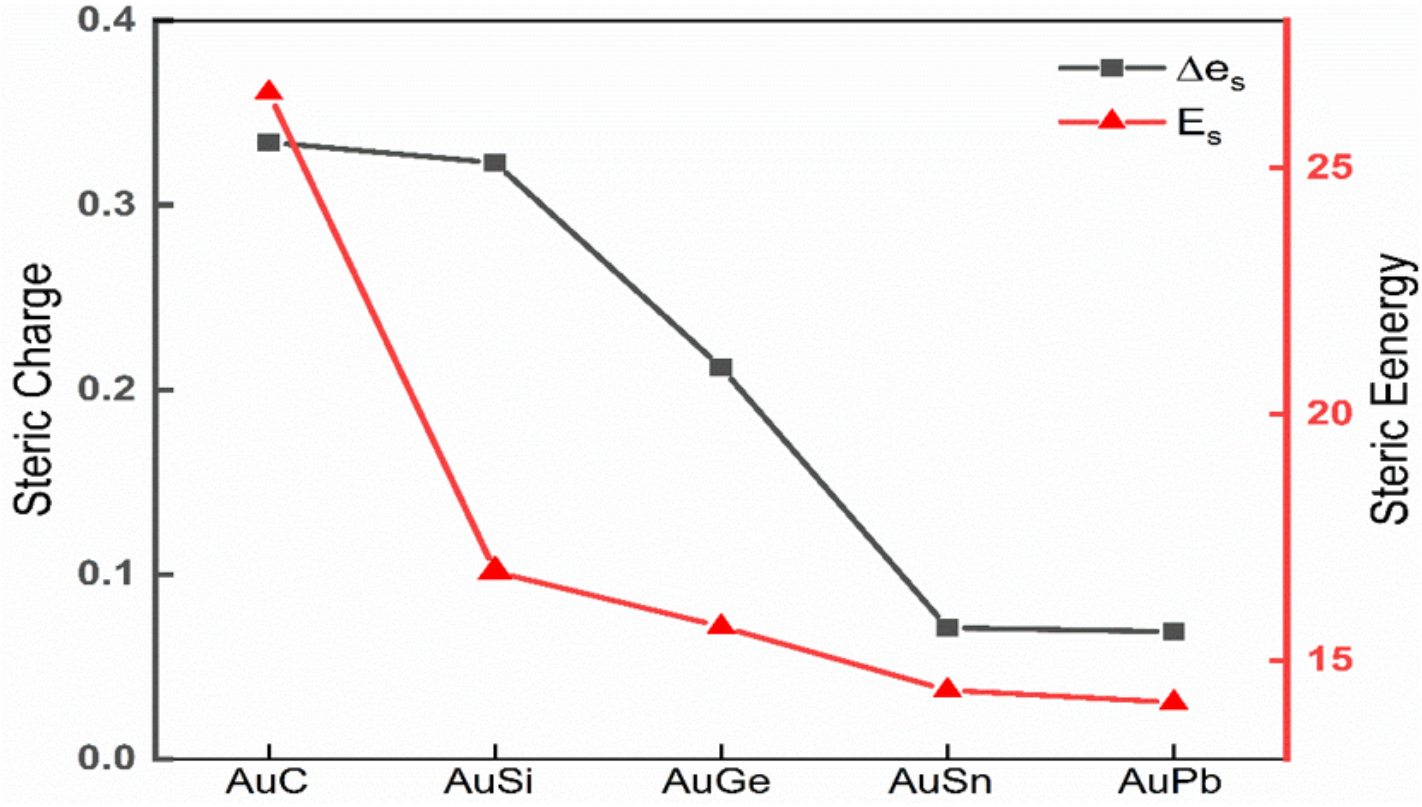

Figure 7

Plots of steric charge deformation on the BCP and corresponding steric energy of AuX systems.